Chinese Chemical Letters 32 (2021) 3435–3439

Contents lists available at ScienceDirect

Chinese Chemical Letters

journal homepage: www.elsevier.com/locate/cclet

Communication

Construction of Cu-Ce interface for boosting toluene oxidation: Study of Cu-Ce interaction and intermediates identified by *in situ* DRIFTS

Jiahui Lu[1], Jinping Zhong[1], Quanming Ren, Jiaqi Li*, Linghe Song, Shengpeng Mo, Mingyuan Zhang, Peirong Chen, Mingli Fu, Daiqi Ye*

School of Environment and Energy, South China University of Technology, Guangzhou 510006, China

ARTICLE INFO

Article history:
Received 4 March 2021
Revised 27 March 2021
Accepted 17 May 2021
Available online 24 May 2021

Keywords:
Cu-Ce interface
Oxygen mobility
Intermediates
In situ DRIFTS
Toluene oxidation

ABSTRACT

A facile hydrothermal method was applied to gain stably and highly efficient CuO-CeO_2 (denoted as Cu1Ce2) catalyst for toluene oxidation. The changes of surface and inter properties on Cu1Ce2 were investigated comparing with pure CeO_2 and pure CuO. The formation of Cu-Ce interface promotes the electron transfer between Cu and Ce through $Cu^{2+} + Ce^{3+} \leftrightarrow Cu^{+} + Ce^{4+}$ and leads to high redox properties and mobility of oxygen species. Thus, the Cu1Ce2 catalyst makes up the shortcoming of CeO_2 and CuO and achieved high catalytic performance with T_{50} = 234 °C and T_{99} = 250 °C (the temperature at which 50% and 90% C_7H_8 conversion is obtained, respectively) for toluene oxidation. Different reaction steps and intermediates for toluene oxidation over Cu1Ce2, CeO_2 and CuO were detected by *in situ* DRIFTS, the fast benzyl species conversion and preferential transformation of benzoates into carbonates through C=C breaking over Cu1Ce2 should accelerate the reaction.

Nowadays, with the rapid development of economy and industry, environmental problems caused by volatile organic compounds (VOCs) emissions have also received increasing attention [1,2]. VOCs includes benzene, toluene, xylene, formaldehyde, *etc.*, as the precursor of $PM_{2.5}$ and a major factor in the generation of O_3, which seriously pollutes the environment and poses a threat to human health [3]. So far, catalytic oxidation is considered to be one of the most effective methods due to its low secondary pollution and high efficiency [4]. Currently, a lot of research has focused on the transition metal oxide catalysts (*e.g.*, MnO_x, Co_3O_4, CeO_2, CuO, ZrO_2) as substitutes for noble metal catalysts because of their low cost and high thermal stability [5–7].

To date, researchers tried to create CuO-CeO_2 mixed oxide catalysts with low cost and high catalytic activity due to the synergistic effect between Cu and Ce. Zeng *et al.* synthesized a highly efficient CuO-CeO_2 catalyst for toluene oxidation by a double redox method, they found that the strong Cu-Ce interaction can promote the electron transfer between CuO and CeO_2 contributes to high redox properties [8]. He *et al.* used a simple self-precipitation protocol to gain mesoporous $CuCeO_x$ catalysts and declared that the Cu^{2+} incorporated into CeO_2 lattice can form the Cu-O-Ce solid solution, which produces large amounts of oxygen vacancies in the interface of CuO and CeO_2 and enhances the catalytic efficiency [9]. Luo *et al.* reported that interaction between CuO and CeO_2 weakens the metal-oxygen bond by sharing oxygen at the interface leading to preferential CO oxidation [10]. Obviously, it has great significance to develop a highly efficient CuO-CeO_2 catalyst and investigate the interaction between CuO and CeO_2. Nevertheless, the catalytic mechanism over CuO-CeO_2 surface, especially VOCs oxidation, is still ambiguous.

It is generally assumed that the catalytic oxidation of VOCs follows the Mars-van Krevelen mechanism [11]. So far, researchers employed *in situ* DRIFTS, GC-MS or TOF-MS to track the key intermediates and by-products to reveal the process of toluene oxidation [12,13]. Yang *et al.* applied *in situ* DRIFTS to track the oxidation process of toluene. They found that toluene adsorbed in the form of benzyl alcohol on the surface of catalysts, then oxidized to benzaldehyde and benzoate species, ring opened to form maleic acid and to final product CO_2 and H_2O [14]. Ye *et al.* used *in situ* DRIFTS and PTR-TOF-MS to study the toluene oxidation process on spinel Co_3O_4 catalysts and suggested the pathway: Toluene, benzyl alcohol, benzaldehyde, benzoate, benzene, phenol, benzoquinone, maleic acid species [13]. Wang *et al.* found that the benzoate could be decomposed into either the carbonates by breaking C=C bond or phenolate by breaking C=O bond, and oxidized to maleic anhydride then finally to CO_2 and H_2O [15]. However, the description

* Corresponding authors.
E-mail addresses: lijiaqi@scut.edu.cn (J. Li), cedqye@scut.edu.cn (D. Ye).
[1] These authors contributed equally to this work.

https://doi.org/10.1016/j.cclet.2021.05.029
1001-8417/

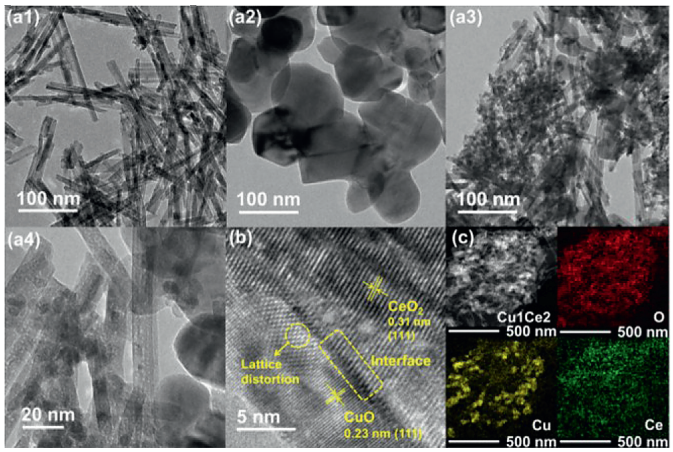

Fig. 1. TEM images of CuO (a1), CeO_2 (a2) and Cu1Ce2 (a3, a4). HRTEM image (b) and EDX analysis mapping (c) of Cu1Ce2.

of the toluene oxidation pathway in literature is divided, it may be due to the reaction path of toluene oxidation related to the properties of catalysts. In our previous work, the oxygen vacancies concentration and crystal phases effects on the reaction step of VOCs oxidation were investigated, we found that these factors have impacts on the activation and generation of products during reaction process [16–18]. However, rarely have the works revealed how the interface affecting the VOCs oxidation pathway.

Inspired by these motivations, herein, CuO was post synthesized and *in-situ* grown on CeO_2 nanorods through a facile hydrothermal method to gain Cu1Ce2 catalysts for toluene oxidation. The characterizations of XRD (powder X-ray diffraction), BET (Brunner-Emmet-Teller measurements), SEM (scanning electron microscope), TEM (transmission electron microscope), Raman (Raman spectra), XPS (X-ray photoelectron spectroscopy), H_2-TPR (H_2-temperature programmed reduction) and O_2-TPD (oxygen temperature programming desorption) were used to study the Cu-Ce interaction on Cu1Ce2 comparing with pure CuO and pure CeO_2. Furthermore, the toluene oxidation mechanism and the reactivity of different adsorbed species over Cu1Ce2, CuO and CeO_2 were investigated by *in situ* DRIFTS.

Fig. S1 (Supporting information) shows the SEM images of the pure CeO_2, CuO, and the Cu-Ce mixed oxide Cu1Ce2. The pure CeO_2 presents nanorod morphology (Fig. S1c) and the pure CuO shows nanoparticle structure (Fig. S1d). As shown in Figs. S1a and b, after growing CuO by hydrothermal method on CeO_2, the CuO particles are bridged on the CeO_2 nanorods forming a matchstick-like morphology. As displayed in Fig. S2 and Table S1 (Supporting information), the nitrogen adsorption-desorption isotherms of the three samples exhibit the type-H3 hysteresis loop which is characteristic of mesoporous materials, broadest pore size distribution and largest pore volume and pore size of Cu1Ce2 are considered to be advantageous to catalytic activity of VOCs oxidation [19,20].

Figs. a1–4a show the TEM images of the three catalysts. The pure CuO particles exist as irregular and large particles with sizes of 50–100 nm, and the pure CeO_2 nanorods present with width of about 8 nm and length of 100–200 nm. However, copper can be found as finely dispersed CuO clusters (less than 5 nm) and bulk CuO particles (up to 30 nm) in Cu1Ce2, indicates CuO were finely dispersed on CeO_2 through the in-situ growing process. It has been reported that small CuO clusters may improve catalytic performance [21]. The high-resolution TEM (HRTEM) image of Cu1Ce2 is exhibited in Fig. 1b, the lattice fringe of 0.31 and 0.23 nm corresponding to the CeO_2 (111) and CuO (111) [8]. Herein, the distortion of CeO_2 lattice can be observed around the interfacial between CuO and CeO_2 phase because of Cu^{2+} incorporation in the CeO_2 lattice [22]. Moreover, EDX mapping images in Fig. 1c show the CuO clusters and bulk CuO particles dispersed on CeO_2.

Fig. 2a shows the XRD diffraction patterns of the three catalysts samples. The phase of CeO_2 and Cu1Ce2 can be attributed to the fluorite structured CeO_2 (PDF No. 43-1002). For the CuO, all diffraction peaks are ascribed to the monoclinic structured CuO (PDF No. 02-1040). It should be pointed out that for the Cu1Ce2, two weak diffraction peaks at 2θ of 35.6° and 38.8° correspond to (−111) and (111) planes for monoclinic CuO can be found [23], and the CeO_2 (111) diffraction peak shift can be observed, indicating the incorporation Cu^{2+} into CeO_2. Herein, as the radius of Cu^{2+} is smaller than that of Ce^{4+}, the incorporation of Cu^{2+} into the CeO_2 framework should cause lattice contraction leading to the peak shifting towards a higher diffraction angle [24].

The surface component over samples and their chemical state were investigated by XPS. As shown in Fig. 2d, for the Ce 3d spectrum, CeO_2 and Cu1Ce2 both present similar profiles and the six peaks marked as V^2, V^3, V^4, U^2, U^3 and U^4 are associated with Ce(IV), while the four peaks marked as V^0, V^1, U^0 and U^1 are related to Ce(III) [25]. As listed in Table S2 (Supporting information), the Ce^{3+} ions ratio for Cu1Ce2 and CeO_2 are 14.1% and 18.8%. With the incorporation of CuO, the Ce^{3+} content on CeO_2 decreased. This phenomenon may be due to the electron transfer from Ce^{3+} to Cu^{2+} through $Cu^{2+} + Ce^{3+} \rightarrow Cu^{+} + Ce^{4+}$ between CuO and CeO_2 [26]. As shown in Fig. 2c, for the Cu1Ce2, the existence of a lower Cu $2p_{3/2}$ peak and the decreased area of satellite peaks are characterized by unsaturated CuO. Meanwhile, a shoulder peak belongs to Cu^{+} can be found in the Cu LMM auger spectra, indicating the CuO on Cu1Ce2 is in the coexistence state of Cu^{+} and Cu^{2+} [26,27]. These results also related to the Cu^{2+} are partially reduced by Ce^{3+}. Quite interestingly, it can be observed that the binding energy of Ce $3d_{2/3}$ over the Cu1Ce2 also shifts to lower value. It may be attributed to electron transfer from Cu^{+} to Ce^{4+} through another redox process: $Cu^{+} + Ce^{4+} \rightarrow Cu^{2+} + Ce^{3+}$. Fig. 2b displays the O 1s XPS spectra of the three samples. Cu1Ce2 exhibits the highest content of surface chemisorbed oxygen and CuO shows the lowest (calculated by $SO_{ads}/(SO_{ads} + SO_{lat})$) (Table S2). This indicates a good agreement between the H_2-TPR O_2-TPD and Raman results in Fig. S3 (Supporting information). Obviously, the construction of Cu-Ce interface can lead to the mobilization of lattice oxygen and promotes the formation of oxygen vacancies.

Fig. S4 (Supporting information) shows the catalytic activity test results of the three catalysts for toluene oxidation under the reaction condition of 1000 ppm toluene, 20% air and weight hourly space velocity (WHSV) 60,000 mL g_{cat}^{-1} h^{-1}. As summarized in Fig. S4 and Table. S3, Cu1Ce2 presents the best catalytic performance with T_{50} = 234 °C, T_{99} = 250 °C (the temperature at which 50% and 90% C_7H_8 conversion is obtained, respectively) among the three catalysts. Notably, the toluene conversion rate for CuO is low in the low temperature stage but increased rapidly in the high temperature stage (T_{50} = 253 °C, T_{99} = 281 °C). However, the different phenomenon can be observed on CeO_2 (T_{50} = 240 °C, T_{99} = 298 °C). Interestingly, Cu1Ce2 obtains the advantages of both CuO and CeO_2 in the high temperature section and low temperature section and shows enhanced catalytic activity. In addition, the long-term activity test in condition of dry air and different relative humidity confirms the excellent catalytic stability of Cu1Ce2 (Fig. S5 in Supporting information).

To understand the reaction mechanism and determine the intermediate species generated of toluene oxidation, *in situ* DRIFTS was employed to reveal the instantaneous composition on the surface of the three different catalysts. All the identified bands and related species are summarized in Table S4 (Supporting information).

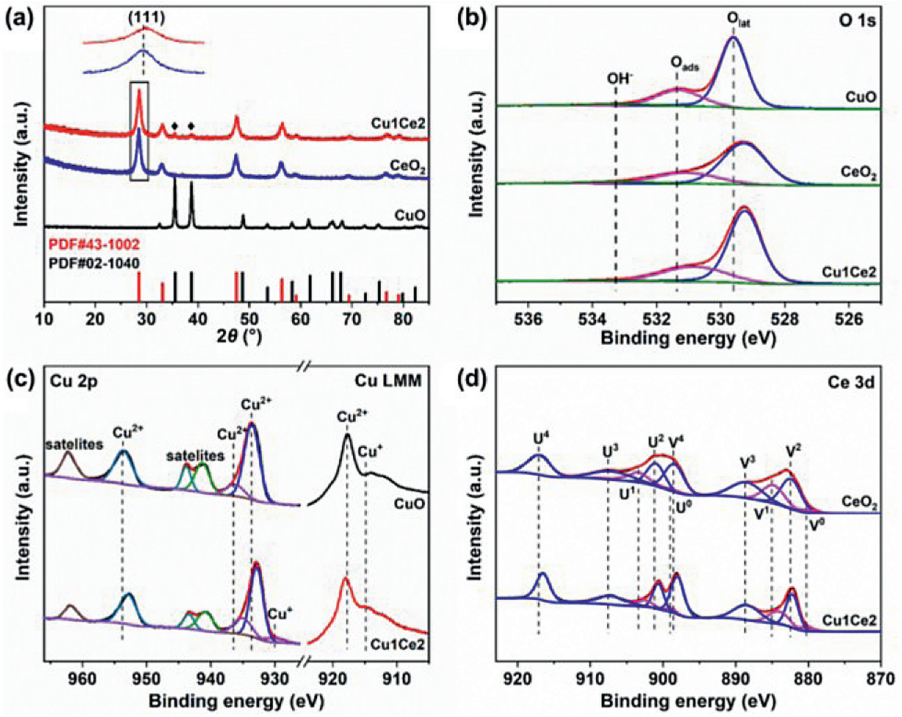

Fig. 2. XRD patterns (a) and XPS spectra of (b) O 1s, (c) Cu 2p and Cu LMM of CuO and Cu1Ce2, (d) Ce 3d of CeO_2 and Cu1Ce2

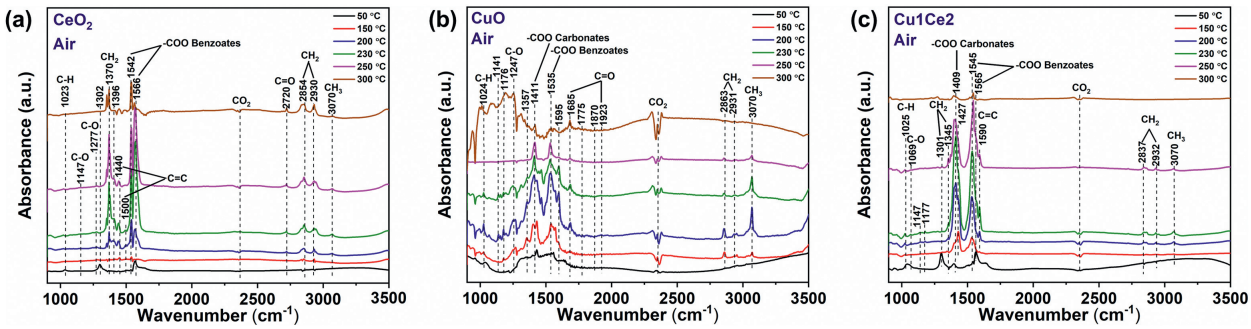

Fig. 3. *In situ* DRIFTS spectra as a function of temperature exposed to 400 ppm toluene/air over CeO_2 (a), CuO (b), Cu1Ce2 (c).

As shown in Fig. 3, the characteristic peaks of major intermediates adsorbed on the surfaces of the three catalysts can be observed from 150 °C, and their intensities reach maximum at 230 °C for CeO_2 and Cu1Ce2, at 200 °C for CuO, then gradually decrease as the temperature continues to increase. In Fig. 3a, for the CeO_2, benzyl species (1370 cm^{-1}) and benzoate species are the major intermediates in the heating period (150–300 °C), the $\upsilon_{(C-H)}$ (2854 cm^{-1}, 2930 cm^{-1}) and $\upsilon_{(C=O)}$ (2720 cm^{-1}) vibrations also confirm with the accumulation of alkoxide species and aldehydic species. As presented in Fig. 3b, for the CuO, carbonate and benzoate species as the major intermediates are observed, and the benzyl species (1147 and 1176 cm^{-1}, alkoxide species; 1685 cm^{-1}, aldehydic species) accumulated as the temperature rose. Remarkably, the adsorption peaks of phenolate species (1247 cm^{-1}) and maleic anhydride species (1700 cm^{-1}– 1950 cm^{-1}) can be found at 150–300 °C, indicating the benzoate species not only convert into carbonates, but also partially transform into phenolate species and then convert into anhydride species on the surface of CuO. Herein, the accumulation of various by-products due to the poor oxygen vacancies and low redox properties of CuO. As shown in Fig. 3c, for the best-performance catalyst Cu1Ce2, carbonate species and benzoate species are the major intermediates in the toluene oxidation process. Meanwhile, there are no obvious adsorption peaks of benzyl species to be observed, confirms that the conversion of benzyl species is promoted over Cu1Ce2. Furthermore, the intensity of carbonate species which are considered as the ring-opened products of toluene, is higher than that of benzoate species at 150–230 °C, and the carbonates decrease rapidly at 250 °C, indicating that benzoate species preferentially transform into carbonates on Cu1Ce2 then convert into H_2O and CO_2. Obviously, toluene can be rapidly adsorbed and activated on the surface of Cu1Ce2. It should be due to the high mobility of oxygen species and abundant oxygen vacancies obtained by the formation of Cu-Ce interface.

Fig. 4 presents the *in situ* DRIFTS of adsorbed surface species arising from Cu1Ce2, CuO to CeO_2 treated with 230 °C in different atmosphere. As shown in Figs. 4a, c, e, in the O-rich atmosphere, most intermediates adsorbed on the three catalysts are similar to the results of temperature-dependent DRIFTS spectra in Fig. 3. Moreover, as presented in Fig. S6 (Supporting information) the growth rate of carbonates on Cu1Ce2 is much higher than the other two catalysts, indicates the C=C breaking of benzoates on Cu1Ce2 is accelerated to form the formation of carbonates. As shown in Figs. 4b, d, f, in the O-poor atmosphere, various intermediates for the three catalysts are further accumulated compar-

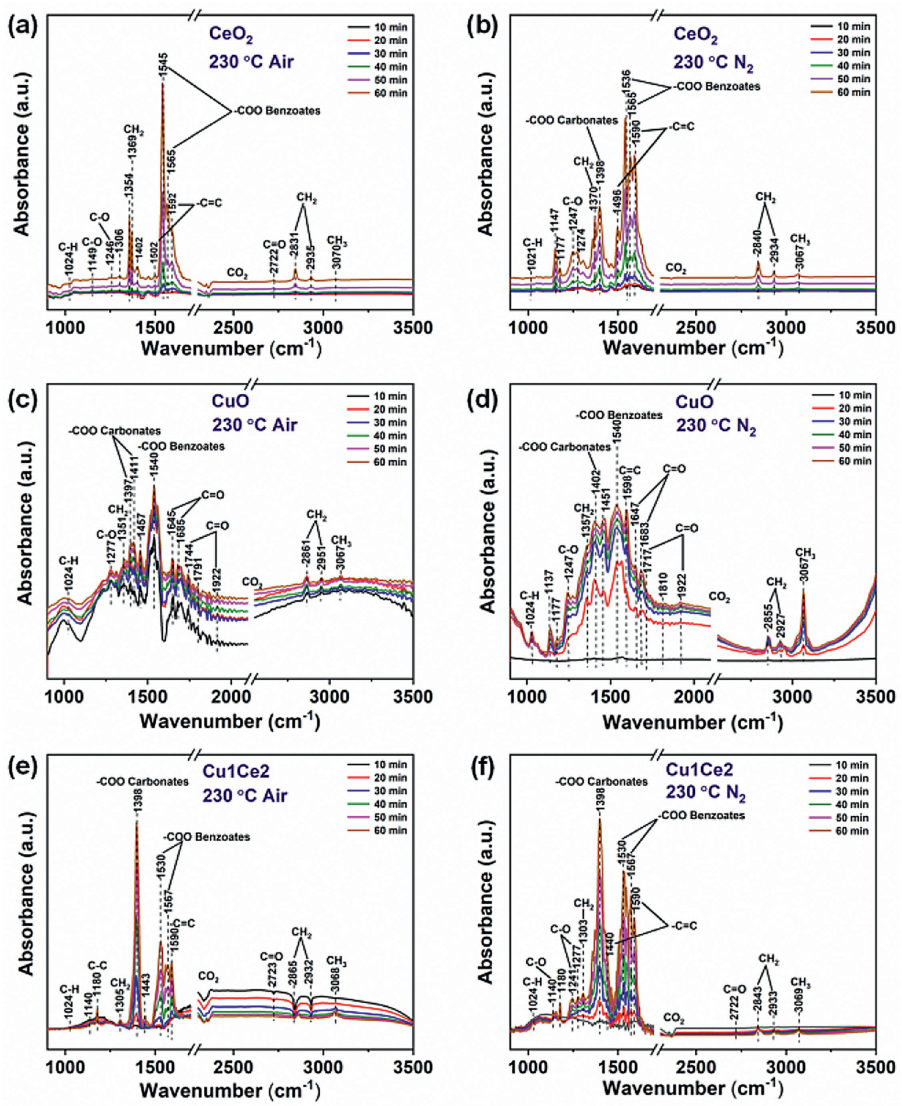

Fig. 4. *In situ* DRIFTS spectra of toluene oxidation as a function of time exposed to toluene 400 ppm/air (a) and toluene 400 ppm/N_2 (b) over CeO_2; Toluene 400 ppm/air (c) and toluene 400 ppm/N_2 (d) over CuO; Toluene 400 ppm/air (e) and toluene 400 ppm/N_2 (f) over Cu1Ce2 at 230 °C.

ing with that under the air atmosphere, implies that the toluene oxidation rate is decreased. It should be due to the oxygen vacancies of catalysts cannot be replenished by gas phase oxygen and reconstruct surface active oxygen species to involve in reaction. In addition, the significant accumulation of carbonates (~1400 cm^{-1}) on the surfaces of the three catalysts indicating that the decomposition of carbonates preferentially to CO_2 and H_2O is prevented in O-poor atmosphere. Hence, typical adsorption peaks of phenolates (~1247 cm^{-1}, ~1277 cm^{-1}) and maleic anhydride species (1700 cm^{-1}– 1950 cm^{-1}) are detected, confirms that the C=C bond of aromatic ring is harder to break in O-poor atmosphere leading to the benzoates partially convert into phenolates, and the phenolates can react with the bulk lattice oxygen to form maleic anhydrides. As presented in Fig. S7 (Supporting information), the low generation rate of phenolates on Cu1Ce2 confirms the C=C bond of aromatic ring can be preferentially broken on Cu1Ce2 even in O-poor atmosphere. As stated above, the C=C breakage of the aromatic ring should be the rate-controlling step during toluene oxidation. Furthermore, combined with the results of XPS, H_2-TPR and O_2-TPD, the formation of Cu-Ce interface is in favor of adsorption and activation for oxygen [8], and the improvement of the migration rate of lattice oxygen and abundant oxygen vacancies leads to the fast C=C breaking of benzoates and accelerating the process of toluene oxidation on Cu1Ce2 [15,16].

Based on these results, the proper mechanism for toluene oxidation on the surface of catalysts is proposed. As shown in Scheme S1 (Supporting information), the oxidation of toluene on the catalysts can be divided into two steps. The first step of toluene oxidation over the three catalysts is consistent: toluene → benzyl alcohol → benzaldehyde → benzoate. In the second step, benzoates are decomposed into carbonates by breaking C=C bond and further converted into H_2O and CO_2 on the CeO_2 and Cu1Ce2. On the surface of the CuO, benzoates can decompose into either the carbonates by breaking C=C bond or phenolate by breaking C=O bond, then further oxidized to anhydride species finally into CO_2 and H_2O. In addition, C=C breakage should be impeded without gas phase oxygen and results in the generation of phenolates and anhydrides. Moreover, the main intermediates on the three catalysts are different: Among them, the main intermediates for Cu1Ce2 are carbonates and partially benzoates; the main intermediate products of CeO_2 are benzoate and part of benzyl substances; The main intermediate products of pure CuO catalyst are benzoate and carbonate, as well as a small amount of benzyl and anhydrides. Thus, the breaking of C=C should be the rate-controlled step in

the toluene oxidation process, and the construction of Cu-Ce interface obtains abundant oxygen vacancies and high mobility of lattice oxygen leading to the rapid benzyl species conversion and speed up the C=C bond breaking of benzoates.

In this work, we reported a facile hydrothermal method to obtain Cu1Ce2 catalysts for toluene oxidation. The formation of Cu-Ce interface affects the phase structure and textural properties of CuO and CeO_2. The Cu-Ce interaction functions through the reaction: $Cu^{2+} + Ce^{3+} \leftrightarrow Cu^{+} + Ce^{4+}$. The enhanced electron transfer between CuO and CeO_2 and the generation of Cu-O-Ce solid solution at the interface lead to high redox properties and abundant oxygen vacancies. Therefore, the Cu1Ce2 catalyst achieves the best catalytic performance both in low and high temperatures with T_{50} = 234 °C and T_{99} = 250 °C. Furthermore, different major intermediates over Cu1Ce2, CeO_2 and CuO were detected by *in situ* DRIFTS: Benzoate and carbonate species over Cu1Ce2; benzyl and benzoate species over CeO_2; benzoate, carbonate and benzyl species over CuO. Herein, the construction of Cu-Ce interface significantly affects the reaction step. The abundant oxygen vacancies and high mobility of lattice oxygen of Cu1Ce2 result in the rapid conversion of benzyl and fast C=C breaking of benzoates to accelerate the toluene oxidation.

Declaration of competing interest

The authors report no declarations of completing interest.

Acknowledgments

This research described above was financially supported by the China Postdoctoral Science Foundation (No. 2018M643090) and the National Natural Science Foundation of China (No. 52000077); the National Key Research and Development Project of Research (No. 2017YFC0212805); the National Natural Science Foundation of China (No. 51878292); the Natural Science Foundation of Guangdong Province, China (No. 2015B020236002); and the China Postdoctoral Science Foundation (No. 2020M682715).

Supplementary materials

Supplementary material associated with this article can be found, in the online version, at doi:10.1016/j.cclet.2021.05.029.

References

[1] M. Zhang, S. Zou, S. Mo, et al., Chemosphere 262 (2021) 127738.
[2] Z. Abbasi, M. Haghighi, E. Fatehifar, et al., J. Hazard. Mater. 186 (2011) 1445–1454.
[3] M. Dezest, M.Le Bechec, L. Chavatte, et al., Sci. Rep. 7 (2017) 10707.
[4] Y.T. Lai, T.C. Chen, Y.K. Lan, et al., ACS Catal. 4 (2014) 3824–3836.
[5] Q. Ren, S. Mo, J. Fan, et al., Chin. J. Catal. 41 (2020) 1873–1883.
[6] M. Zhang, S. Zou, Q. Zhang, et al., Inorg. Chem. 59 (2020) 3062–3071.
[7] J. Wang, X. Quan, S. Chen, et al., J. Hazard. Mater. 368 (2019) 621–629.
[8] Y. Zeng, K.G. Haw, Z. Wang, et al., J. Hazard. Mater. 404 (2021) 124088.
[9] C. He, Y. Yu, L. Yue, et al., Appl. Catal. B: Environ. 147 (2014) 156–166.
[10] J.Y. Luo, M. Meng, Y.Q. Zha, L.H. Guo, J. Phys. Chem. C 112 (2008) 8694–8701.
[11] C. He, J. Cheng, X. Zhang, et al., Chem. Rev. 119 (2019) 4471–4568.
[12] W. Xu, B. Chen, X. Jiang, et al., J. Hazard. Mater. 387 (2020) 122004.
[13] J. Zhong, Y. Zeng, D. Chen, et al., J. Hazard. Mater. 386 (2020) 121957.
[14] X. Yang, X. Yu, M. Jing, et al., ACS Appl. Mater. Interfaces 11 (2019) 730–739.
[15] P. Wang, J. Wang, X. An, et al., Appl. Catal. B: Environ. 282 (2021) 119560.
[16] S. Mo, Q. Zhang, J. Li, et al., Appl. Catal. B: Environ. 264 (2020) 118464.
[17] Q. Zhang, S. Mo, J. Li, et al., Catal. Sci. Technol. 9 (2019) 4538–4551.
[18] J. Fan, Q. Ren, S. Mo, et al., ChemCatChem 12 (2020) 1046–1054.
[19] W. Xu, X. Chen, J. Chen, H. Jia, J. Hazard. Mater. 403 (2021) 123869.
[20] X. Zhang, H. Zhao, Z. Song, et al., Appl. Surf. Sci. 493 (2019) 9–17.
[21] M. Zabilskiy, P. Djinović, B. Erjavec, G. Dražić, A. Pintar, Appl. Catal. B Environ. 163 (2015) 113–122.
[22] S. Zeng, K. Liu, L. Zhang, et al., J. Power Sources 261 (2014) 46–54.
[23] S. Zeng, Y. Wang, B. Qin, et al., Catal. Sci. Technol. 3 (2013) 3163–3172.
[24] S.T. Hossain, E. Azeeva, K. Zhang, et al., Appl. Surf. Sci. 455 (2018) 132–143.
[25] R. Peng, S. Li, X. Sun, et al., Appl. Catal. B Environ. 220 (2018) 462–470.
[26] Y. Zeng, Y. Wang, F. Song, S. Zhang, Q. Zhong, Sci. Total Environ. 712 (2020) 135635.
[27] Y. Xia, J. Lao, J. Ye, et al., ACS Sustain. Chem. Eng. 7 (2019) 18421–18433.